External field effects on dielectronic recombination rate coefficients for oxygen atomic ions

P. Krylstedt* and M. S. Pindzola

Department of Physics, Auburn University, Auburn, Alabama 36849-5311

N. R. Badnell[†]

AWE, Aldermaston, Reading, RG7 4PR, United Kingdom

(Received 4 August 1989)

The effects of external electric fields on $\Delta n = 0$ dielectronic recombination (DR) rate coefficients for O^{q+}, $q = 1, \ldots, 5$ are calculated using a configuration-average distorted-wave approach. Field-ionization effects lead to a decrease in the DR rate coefficient while field-mixing effects lead to an increase in the DR rate coefficient. Overall, strong fields produce a significant decrease in the DR rate coefficient at the peak temperature, i.e., by over a factor of 10 for several oxygen ions. The configuration-average distorted-wave results are also compared with the Burgess general formula II [A. Burgess (private communication)] that includes both field-mixing and ionization effects. It is found that this formula roughly models these effects, and some guidelines as to the range of validity of this simple-to-use formula are developed. In the limit of zero external electric fields, the distorted-wave approach is further compared with recent sophisticated configuration-mixing intermediate-coupling calculations as well as with the Burgess general formula I [A. Burgess, Astrophys. J. **141**, 1588 (1965)].

I. INTRODUCTION

Environmental effects play a prominent role in the modeling of various plasma conditions and are thus of importance to thermonuclear fusion research.[1] In the present paper we are interested in the investigation of the impact of external electric fields on dielectronic recombination (DR) processes occurring in low-density plasmas. Electric field effects lead to both an increase in the DR rate coefficients due to Rydberg-state mixing, which opens up new recombination channels, and a decrease in the DR rate coefficients due to field ionization.[2,3] In order to explore this fact we have employed a configuration-average distorted-wave (CADW) method including both field effects to calculate $\Delta n = 0$ DR rate coefficients for oxygen atomic ions. The CADW approximation should be suitable for this study, although special care should always be exercised when facing certain pathological cases. In fact, we have found that O^{4+} constitutes such a difficult system for the CADW model.

In a previous contribution[4] we carried out configuration-mixing intermediate-coupling (IC) calculations in the zero-field limit using the program AUTOSTRUCTURE,[5] and partitioned configuration-average calculations in the case of maximum-field enhancement as well as in the zero-field limit using a modified version of the program DRACULA.[6] We concentrated on the DR cross sections of $\Delta n = 0$ core transitions in the oxygen isonuclear sequence. The results were also compared with data from a number of recent experiments.[7−9] In the current contribution we present DR rate coefficients

for the same ions using a similar calculational approach. The configuration-average distorted-wave results including field-mixing and ionization effects are also compared with data obtained using the Burgess general formula II (Ref. 10) (GFII). The GFII provides DR rate coefficients that agree qualitatively with the CADW results. However, quantitatively they may be off by more than an order of magnitude at the peak temperature. Furthermore, the field-free CADW results are compared with the IC data and with the general formula I of Burgess[11] (GFI). In some sense, this provides a test of the relevance of employing the configuration-average distorted-wave approximation for this case as well as a viable test of the applicability of the two formulas of Burgess for a wide range of charge states.

In Sec. II we outline very briefly the theory behind the intermediate-coupling and the configuration-average distorted-wave calculations. In particular, we discuss the implementation of field effects into the CADW approximation. We also give some information about the GFI and the GFII. This is done in some detail since the latter has not been discussed in the general literature before. In Sec. III we present our results and discuss some possible implications for fusion research in general as well as the applicability of the GFI and the GFII. We summarize the paper in Sec. IV by giving some concluding remarks.

II. THEORY

The energy-averaged dielectronic recombination cross section for a given initial state i through an intermediate state j is given by[12]

$$\bar{\sigma}_{DR}(i;j) = \frac{(2\pi a_0 I_H)^2}{E_c \Delta E_c} \frac{g_j}{2g_i} \frac{\tau_0 \sum_k A_r(j \to k) \sum_l A_a(j \to i, E_c l)}{\sum_h [A_r(j \to h) + \sum_l A_a(j \to h, E_c l)]} ,$$ (1)

where E_c is the energy of the continuum electron, ΔE_c is the bin width, and I_H is the ionization potential of hydrogen (all in the same units of energy). g_j and g_i are the statistical weights of the $(N+1)$-electron doubly excited level and the N-electron target-ion level, respectively. The rates are given in units of inverse seconds and $(2\pi a_0)^2 \tau_0 = 2.6741 \times 10^{-32}$ cm^2 sec. However, employing the configuration-average distorted-wave approximation, the energy-averaged dielectronic-recombination cross section can be written[6]

$$\bar{\sigma}_{DR}^{CA}(I;J) = \frac{(2\pi a_0 I_H)^2}{E_c \Delta E_c} \frac{G_J}{2G_I} \frac{\tau_0 \bar{A}_a(J \to I) \sum_K \bar{A}_r(J \to K)}{\sum_H [\bar{A}_a(J \to H) + \bar{A}_r(J \to H)]} ,$$ (2)

i.e., obtained from an interpolation between the two limiting cases of dominance of the radiative rates and the autoionizing rates, respectively. Here G_J and G_I are the *total* statistical weights of the doubly excited *configuration* and the initial *configuration*, respectively, and the sums are over configurations instead of levels. In passing we note that the configuration-average approximation for DR cross sections will not be very accurate in cases for which the sum of the individual autoionizing rates and the sum of the individual radiative rates are comparable. The total dielectronic recombination rate coefficient may be written in terms of the energy-averaged cross section $\bar{\sigma}_{DR}$ or $\bar{\sigma}_{DR}^{CA}$ as[12]

$$\alpha_{DR}(\mathcal{J};\text{tot}) = \left[\frac{4\pi a_0^2 I_H}{k_b T} \right]^{3/2} \frac{1}{(2\pi a_0 I_H)^2 \tau_0}$$

$$\times \sum_{\mathcal{J}} E_c \Delta E_c \bar{\sigma}(\mathcal{J}; \mathcal{J}) e^{-E_c/k_b T} ,$$ (3)

where $(4\pi a_0^2)^{3/2} = 6.6011 \times 10^{-24}$ cm^3, and $\mathcal{J}$ and $\mathcal{J}$ denote levels or configurations. The equations may be evaluated in the configuration-mixing intermediate coupling approximation using the program AUTOSTRUCTURE and in the CADW approximation employing DRACULA.

In the configuration-average distorted-wave approximation the influence of field effects can be modeled by a Clebsch-Gordan transformation of the autoionizing rates, for a fixed n value, from spherical to parabolic coordinates,[6] i.e.,

$$|nkm\rangle = \sum_{l=|m|}^{n-1} (C_{(m-k)/2(m+k)/2}^{(n-1)/2 (n-1)/2 \ l} {}_m)|nlm\rangle ,$$ (4)

where $C_{(m-k)/2(m+k)/2}^{(n-1)/2 (n-1)/2 \ l} {}_m$ is the Clebsch-Gordan coefficient and k is the electric quantum number defined as $k = n_1 - n_2$, where n_1 and n_2 are the parabolic quantum numbers given by $n = n_1 + n_2 + |m| + 1$. When ex-

change is neglected, the configuration-average autoionizing rates then transform as

$$\bar{A}_a(n,k,m) = \sum_{l=|m|}^{n-1} |C_{(m-k)/2(m+k)/2}^{(n-1)/2 (n-1)/2 \ l} {}_m|^2 \bar{A}_a(n,l) .$$ (5)

In general, when exchange is included, cross terms will appear in Eq. (5). However, for the present application, we have used the transformation (5) with exchange incorporated in the rates. Together with the corresponding transformation of the radiative rates this will model the DR rate coefficients subject to Rydberg-state mixing. The decrease in the DR rate coefficients caused by field ionization may be incorporated in the CADW approximation by adding a field ionization rate to the sum over rates in the denominator of Eq. (2). However, field ionization rates tend to be very small until one reaches a critical value of n, at which point the rate increases dramatically. Thus we will include all Rydberg states up to a maximum principal quantum number n_{max} determined from the following semiclassical field-ionization formula

$$n_{max} = (6.2 \times 10^8 q^3/F)^{1/4} ,$$ (6)

where q is the charge of the ion before recombination and F is the electric field in V/cm. This semiclassical equation is based on a comparison of quantum-mechanical tunneling with radiative decay, and its validity has been investigated by Bottcher, Griffin, and Pindzola[13] using the formalism of Damburg and Kolosov[14] and Lanczos.[15]

In order to make very rapid overall surveys of recombination processes, Burgess[11] has derived a well-known rather simple-to-use general formula for DR rate coefficients in the limit of zero external electric fields. In order to include the field effects discussed above, this general formula may be modified according to[10]

$$\alpha_{DR}^{GFII}(i,\text{tot}) = \frac{8}{T^{3/2}} \sum_{n=n_0}^{n_{max}} \frac{Z^2}{n^3} \sum_j \frac{f(i,j)}{E_{ij}/I_H} \frac{\exp-(E_{ij}/\{1+0.015[Z^3/(Z+1)^2]\}k_b T)}{[1+2\times 10^6 Z^2/n^5(E_{ij}/I_H)^3]} ,$$ (7)

where i and j denote the initial target state and the intermediate (core) state, respectively. Z is the charge on the target ion, E_{ij} is the core excitation energy, T is the electron temperature, I_H is the ionization potential of H, $f(i,j)$ is the upward oscillator strength, and n_{max} is coupled to the charge of the ion (before recombination) and the electric field strength as given in Eq. (6). The Burgess general formula II models the statistical population of l states produced by strong perturbations such as, for instance, external fields, however, it does not model autoionization into excited states.

III. RESULTS AND DISCUSSION

In Figs. 1(a)–5(a) we display our theoretical configuration-average distorted-wave DR rate coefficient results for O^{q+}, $q = 1, \ldots, 5$, and for various values of cutoff in the principal quantum number due to field-ionization. For example, for O^+ a cutoff at $n = 20$ corre-

sponds to a field strength of 4 kV/cm. The shaded areas in Figs. 1(a)–5(a) represent the domains enclosed by the zero-field rates and the maximum field enhancement results for the various cases. Electric field effects lead to both an increase in the DR rate coefficients due to Rydberg-state mixing and a decrease in the DR rate coefficients due to field ionization. It is thus of interest to note that although a certain analyzing field strength will introduce a cutoff in n, electric fields in the interaction region will still produce an enhancement in the DR rate coefficients associated with the lower n values, i.e., below the current n_{max}. Figures 1(a)–5(a) are produced in order to stress and explore this fact. Hence, for each value of cutoff in n, we obtain approximate upper and lower bounds for the DR rate coefficients, and by displaying results for different values of n_{max} we also explore the parameter space of the configuration-average distorted-wave method. The former claim is also supported by earlier comparisons with experimental results on Na-like[16]
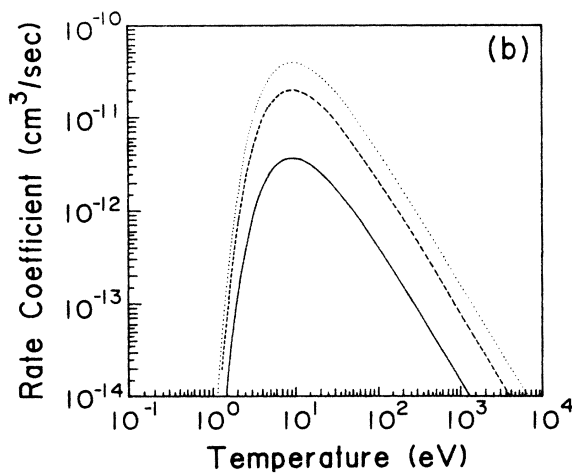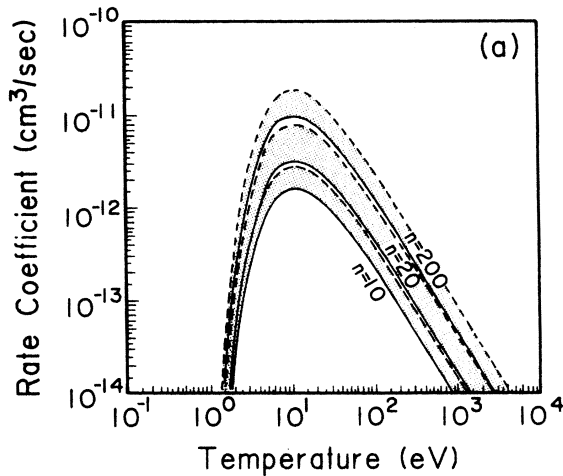

FIG. 1. (a) CADW zero-field and maximum-field enhancement O^+ dielectronic recombination rate coefficients as a function of the temperature. Displayed are the results for $n_{max} = 10, 20, 200$. (b) The same as in (a) but obtained from the Burgess general formula II. Shown are the results for $n_{max} = 10$, solid curve; 20, dashed curve; and 200, dotted curve.
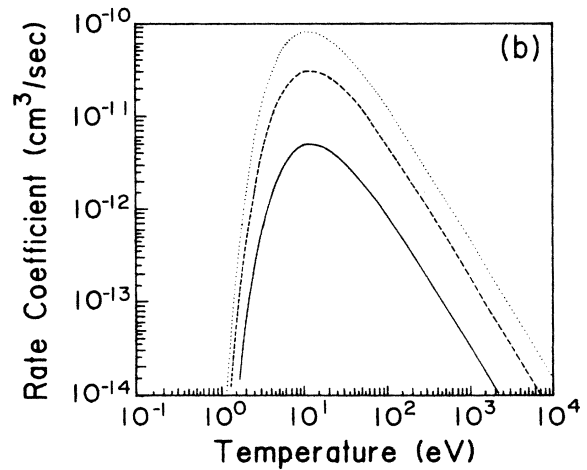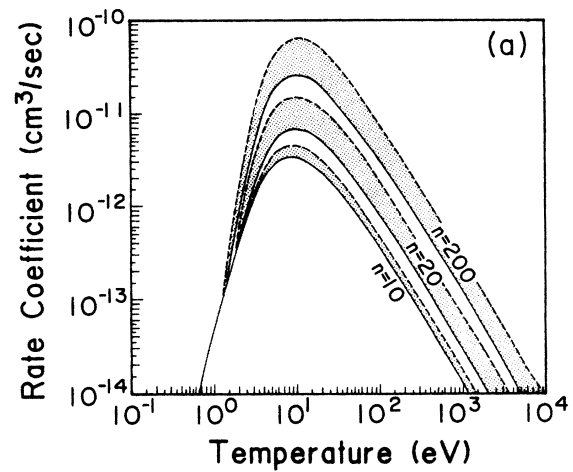
FIG. 2. (a) CADW zero-field and maximum-field enhancement O^{2+} dielectronic recombination rate coefficients as a function of the temperature. Displayed are the results for $n_{max} = 10, 20, 200$. (b) The same as in (a) but obtained from the Burgess general formula II. Shown are the results for $n_{max} = 10$, solid curve; 20, dashed curve; and 200, dotted curve.

and Be-like[8] ions as well as with experimental data for O^{3+}.[4] In Figs. 1(b)–5(b) we show the corresponding field enhanced DR rate coefficients for O^{q+}, $q = 1, \ldots, 5$, obtained from the Burgess general formula II for the same values of n cutoff as used in the CADW calculations. The GFII results were obtained using core excitation energies and oscillator strengths from Wiese, Smith, and Glennon[17] (the National Standard Reference Data Series tables of atomic transition probabilities).

From Figs. 1(a) and 1(b) we see that the overall qualitative agreement between the CADW results and the GFII data for O^+ is rather good. However, the GFII predicts a higher maximum value for the rate coefficient than the CADW method. It also places the maximum at a slightly lower temperature as compared with the CADW method. This is especially true for the low n-cutoff case, while the results for larger n_{max} values seem to converge. This is consistent with the fact that the Burgess formulas are deduced from low-density data. Hence, as the field strength increases, we expect to see a deviation from the CADW results. A comparison of Figs. 2(a) and 2(b) shows the same general features as the previous case, but the assignment of the maximum is here the opposite, i.e., the CADW method predicts it to occur at the lower temperatures. The discrepancies in the predicted peak values have further decreased for the present ion. Hence the O^{2+} results differ in this sense from the O^+ data. From Figs. 3(a) and 3(b) we observe that the CADW and GFII results agree quite well for the low and high n_{max} values in the case of O^{3+}. However, for the intermediate n_{max} value the GFII produces a maximum rate coefficient which is significantly larger than the corresponding
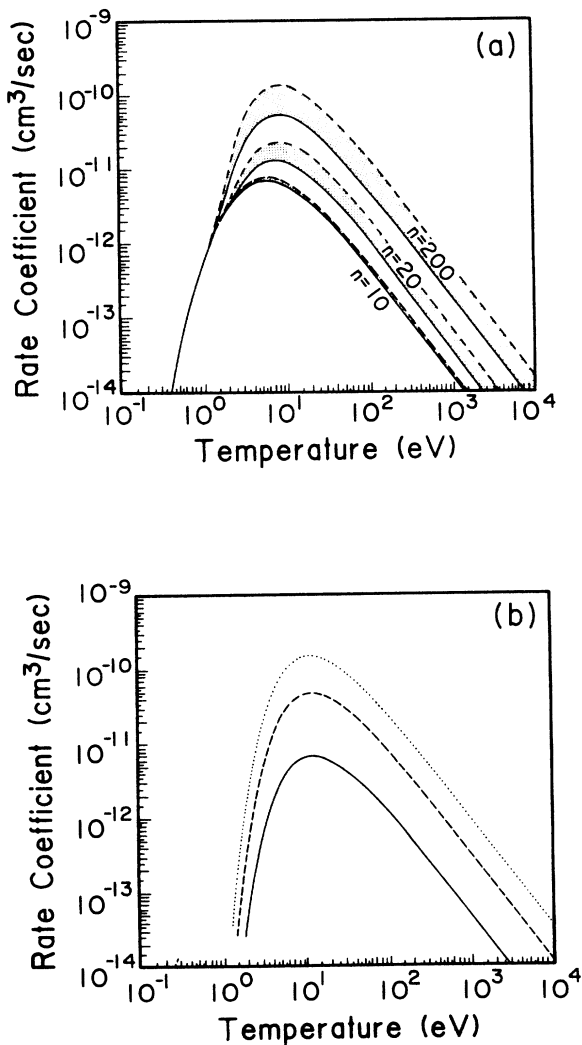

FIG. 3. (a) CADW zero-field and maximum-field enhancement O^{3+} dielectronic recombination rate coefficients as a function of the temperature. Displayed are the results for $n_{max} = 10, 20, 200$. (b) The same as in (a) but obtained from the Burgess general formula II. Shown are the results for $n_{max} = 10$, solid curve; 20, dashed curve; and 200, dotted curve.
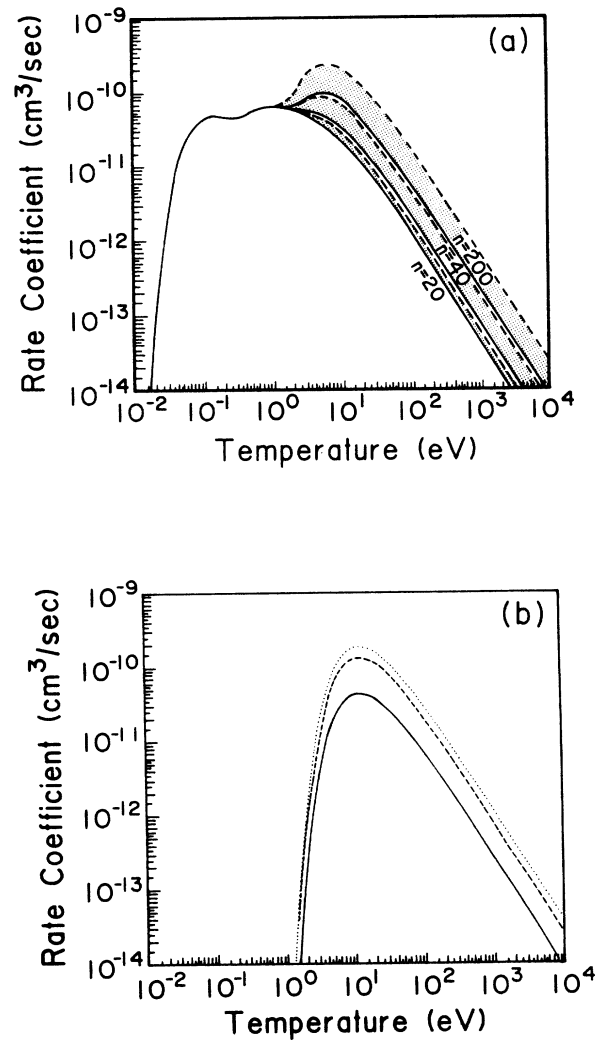
FIG. 4. (a) CADW zero-field and maximum-field enhancement O^{4+} dielectronic recombination rate coefficients as a function of the temperature. Displayed are the results for $n_{max} = 20, 40, 200$. (b) The same as in (a) but obtained from the Burgess general formula II. Shown are the results for $n_{max} = 20$, solid curve; 40, dashed curve; and 200, dotted curve.

CADW result. The GFII further places the maxima at somewhat higher temperatures than the CADW method, but the discrepancies decrease for the higher n-cutoff values. This agrees with the observations made in the O^{2+} case.

From Figs. 1(a)–3(a) we see that the shaded areas tend to separate as we go to higher charge states. Note also that the shaded domain associated with the low cutoff results shrinks along the isonuclear sequence, while the corresponding large n_{max} region stays relatively constant. The intermediate cutoff results also shrink somewhat, but far from the rate of the low n_{max} data. This effect on the low cutoff results may be explained by considering the fact that intermediate doubly excited states become bound as we go to higher charge states. Hence, for the low n_{max} case, the relative depletion of possible inter-

mediate states grows rapidly whereas the effect on the higher n_{max} cases is not that dramatic. Note further that for low temperatures DR rate coefficients are dominated by contributions from low-lying states. This is due to the exponential factor in Eq. (3), which tends to cutoff the full Rydberg series.

From Figs. 4(a) and 4(b) we see that the O^{4+} results obtained by the GFII and CADW method agree relatively well for higher temperatures. However, for lower temperatures the CADW rate coefficients stay rather constant while the corresponding GFII data fall off rather rapidly. Note that the CADW results eventually decrease for even lower temperatures. This behavior is an "artifact" created by the configuration-average approximation in this case. O^{4+} is a Be-like ion with ground-state configuration $1s^2 2s^2 (^1S)$. The DR takes place via capture into the doubly excited $2s2p\,(^1P)nl$ and $2s2p\,(^3P)n'l'$ states which may subsequently stabilize by radiative transitions to lower states. The ^1P to ^1S transition is a spin-allowed transition whereas the ^3P to ^1S is spin forbidden. However, the CADW method mixes in the ^3P states in the sense that it calculates a configuration-average state from the ^1P and ^3P states. This average level (with a set of Rydberg states attached to it) will end up somewhere between the two original states, i.e., closer to the ^3P than the ^1P. This will create the low-temperature structures seen in Fig. 4(a) and also shift the peak values toward lower temperatures. Thus no real significance should be attached to these low-temperature structures. For the O^{5+} case displayed in Figs. 5(a) and 5(b) we observe very good agreement between the results of the two models for the higher values of cutoff while the low n_{max} data show some discrepancies. In passing we note that the DR rate coefficients scale as $T^{-3/2}$ for high values of the temperature. Hence this may be used in order to extrapolate DR rate coefficients for even higher temperatures. We have also observed the effect of increasing ionicity in the sense that the overall maximum value of the DR rate coefficient increases with Z along the O isonuclear sequence. In closing this comparison we note that the inclusion of the valence-electron radiative transitions, as discussed in the next paragraph, in the CADW model tends to emphasize the transitions associated with lower temperatures, and that the GFII does not model these transitions. Hence, taking this fact into account, the Burgess general formula II seems to produce, qualitatively, rather good DR rate coefficients for the currently examined ions. However, quantitatively the GFII rate coefficients may be off by a factor of 2 to 3. From Figs. 1(a)–5(a) we also observe that for small field strengths the overall effects are to produce an increase in the DR rate coefficient while for strong fields the DR rate coefficients ultimately drop by over a factor of 10 (as compared with the field-free rates) for the currently investigated ions. Furthermore, electric fields are also seen to alter the position of the maximum in the DR rate coefficients. We have thus found that environmental effects can make a substantial impact on the DR process. This certainly suggests that an appropriate description of different environmental conditions is vital to the understanding of dynamical processes occurring in
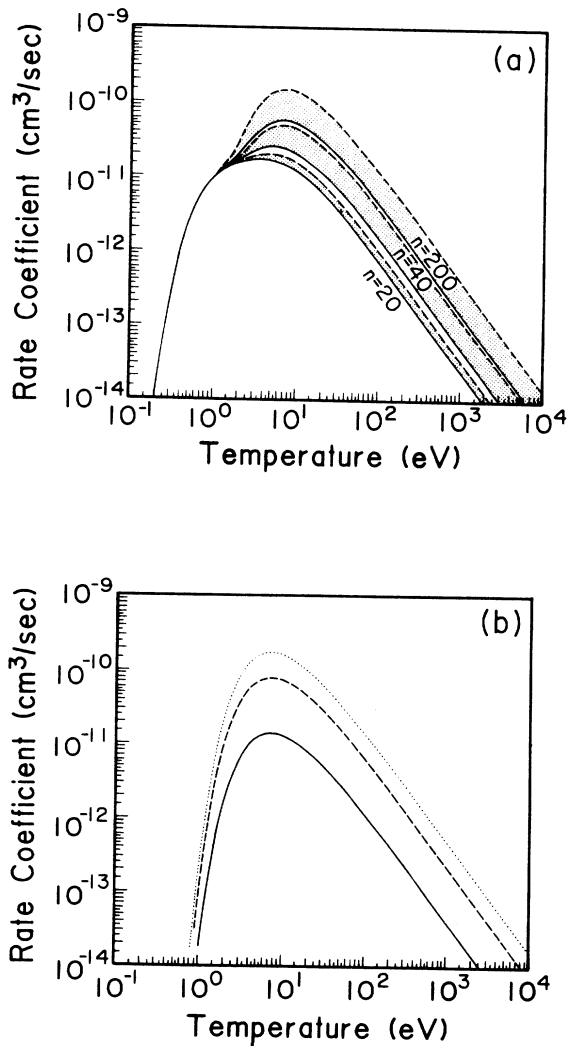

FIG. 5. (a) CADW zero-field and maximum-field enhancement O^{5+} dielectronic recombination rate coefficients as a function of the temperature. Displayed are the results for $n_{max} = 20, 40, 200$. (b) The same as in (a) but obtained from the Burgess general formula II. Shown are the results for $n_{max} = 20$, solid curve; 40, dashed curve; and 200, dotted curve.

TABLE I. Dielectronic recombination rate coefficients (cm^3/s) for O^+ obtained from the GFI and the CADW and IC methods in the limit of zero external electric field.

$\log_{10}T$ (K)	GFI	O^+ CADW	IC
4.6	2.24×10^{-12}	1.40×10^{-12}	1.62×10^{-12}
4.8	5.53×10^{-12}	4.35×10^{-12}	4.33×10^{-12}
5.0	7.58×10^{-12}	6.92×10^{-12}	6.26×10^{-12}
5.2	7.17×10^{-12}	7.18×10^{-12}	6.12×10^{-12}
5.4	5.36×10^{-12}	5.70×10^{-12}	4.68×10^{-12}
5.6	3.46×10^{-12}	3.82×10^{-12}	3.06×10^{-12}
5.8	2.03×10^{-12}	2.30×10^{-12}	1.82×10^{-12}
6.0	1.13×10^{-12}	1.29×10^{-12}	1.01×10^{-12}
6.2	6.02×10^{-13}	6.97×10^{-13}	5.42×10^{-13}
6.4	3.14×10^{-13}	3.66×10^{-13}	2.84×10^{-13}
6.6	1.61×10^{-13}	1.89×10^{-13}	1.46×10^{-13}
6.8	8.22×10^{-14}	9.64×10^{-14}	7.44×10^{-14}

various plasmas.

In order to attempt to justify the use of the CADW approximation (when studying the impact of environmental effects on DR processes), we will now compare the CADW data with sophisticated configuration-mixing intermediate-coupling results for the field free case. In Tables I–V we present DR rate coefficients for O^{q+}, $q = 1, \ldots, 5$, obtained from the Burgess general formula I, and the CADW and IC methods in the limit of zero external electric fields. The CADW results were obtained by including Rydberg states up to a maximum value of n and l given by 200 and 19, respectively. The IC data are taken from Ref. 4. The GFI rate coefficients were obtained using core excitation energies and oscillator strengths from Ref. 17. Both the GFI and the CADW method give results that are in rather good agreement with the IC data. The discrepancies are mainly attributed to the fact that the GFI does not model autoionization into excited states. Note that the GFI was deduced from low-density plasma data and is supposed to be valid for low Z, i.e., $1 \leq Z \leq 20$. Hence we expect the GFI to slightly overestimate the DR rate coefficients for the O isonuclear sequence. The limitations of the CADW model were discussed above and will not be repeated here. However, although the current case is the field-free limit, we note that in discussing DR one usually distinguishes between two types of radiative transitions. The first type includes those in which the Rydberg electron is a spectator, and the rates are nearly independent of n and l. In the second type the Rydberg electron is the active electron, and the rates are highly dependent on the values of n and l. The IC results of Ref. 4 were obtained without these Rydberg electron transitions. However, the overall effect of this approximation on DR rate coefficients should be less than 5% whereas the impact on DR cross sections may be considerably larger. We also note that DR takes place through the Rydberg series attached to a single core term for O^+, O^{4+}, and O^{5+}, but through more than one core term for O^{2+} and O^{3+}.

From Table I we have that the GFI and CADW results for the maximum value of the DR rate coefficient for O^+ are a factor of 1.2 and 1.1 larger than the IC data, respectively. Note that the CADW model places the maximum at a somewhat higher temperature than the IC model while the GFI predicts a maximum at approximately the same temperature as the IC method. We also observe

TABLE II. Dielectronic recombination rate coefficients (cm^3/s) for O^{2+} obtained from the GFI and the CADW and IC methods in the limit of zero external electric field.

$\log_{10}T$ (K)	GFI	O^{2+} CADW	IC
4.6	4.06×10^{-12}	7.12×10^{-12}	3.65×10^{-12}
4.8	1.21×10^{-11}	1.79×10^{-11}	1.08×10^{-11}
5.0	1.97×10^{-11}	2.52×10^{-11}	1.78×10^{-11}
5.2	2.13×10^{-11}	2.43×10^{-11}	1.96×10^{-11}
5.4	1.76×10^{-11}	1.84×10^{-11}	1.65×10^{-11}
5.6	1.22×10^{-11}	1.20×10^{-11}	1.15×10^{-11}
5.8	7.49×10^{-12}	7.09×10^{-12}	7.14×10^{-12}
6.0	4.27×10^{-12}	3.94×10^{-12}	4.10×10^{-12}
6.2	2.33×10^{-12}	2.11×10^{-12}	2.24×10^{-12}
6.4	1.23×10^{-12}	1.10×10^{-12}	1.19×10^{-12}
6.6	6.36×10^{-13}	5.67×10^{-13}	6.15×10^{-13}
6.8	3.26×10^{-13}	2.89×10^{-13}	3.15×10^{-13}

TABLE III. Dielectronic recombination rate coefficients (cm³/s) for O^{3+} obtained from the GFI and the CADW and IC methods in the limit of zero external electric field.

$\log_{10}T$ (K)	GFI	O^{3+} CADW	IC
4.6	6.53×10^{-12}	2.44×10^{-11}	5.61×10^{-12}
4.8	2.30×10^{-11}	4.61×10^{-11}	1.73×10^{-11}
5.0	4.17×10^{-11}	5.46×10^{-11}	3.20×10^{-11}
5.2	4.80×10^{-11}	4.74×10^{-11}	3.80×10^{-11}
5.4	4.10×10^{-11}	3.37×10^{-11}	3.33×10^{-11}
5.6	2.88×10^{-11}	2.10×10^{-11}	2.39×10^{-11}
5.8	1.79×10^{-11}	1.21×10^{-11}	1.50×10^{-11}
6.0	1.03×10^{-11}	6.63×10^{-12}	8.69×10^{-12}
6.2	5.62×10^{-12}	3.51×10^{-12}	4.77×10^{-12}
6.4	2.97×10^{-12}	1.82×10^{-12}	2.53×10^{-12}
6.6	1.54×10^{-12}	9.34×10^{-13}	1.32×10^{-12}
6.8	7.90×10^{-13}	4.75×10^{-13}	6.75×10^{-13}

TABLE IV. Dielectronic recombination rate coefficients (cm³/s) for O^{4+} obtained from the GFI and the CADW and IC methods in the limit of zero external electric field.

$\log_{10}T$ (K)	GFI	O^{4+} CADW	IC
4.6	8.53×10^{-12}	8.44×10^{-11}	3.79×10^{-11}
4.8	3.29×10^{-11}	9.46×10^{-11}	4.36×10^{-11}
5.0	5.98×10^{-11}	8.47×10^{-11}	5.17×10^{-11}
5.2	6.75×10^{-11}	6.24×10^{-11}	5.05×10^{-11}
5.4	5.65×10^{-11}	4.02×10^{-11}	4.02×10^{-11}
5.6	3.91×10^{-11}	2.36×10^{-11}	2.74×10^{-11}
5.8	2.41×10^{-11}	1.31×10^{-11}	1.68×10^{-11}
6.0	1.37×10^{-11}	7.00×10^{-12}	9.61×10^{-12}
6.2	7.46×10^{-12}	3.66×10^{-12}	5.15×10^{-12}
6.4	3.93×10^{-12}	1.88×10^{-12}	2.68×10^{-12}
6.6	2.04×10^{-12}	9.57×10^{-13}	1.36×10^{-12}
6.8	1.04×10^{-12}	4.85×10^{-13}	6.85×10^{-13}

TABLE V. Dielectronic recombination rate coefficients (cm³/s) for O^{5+} obtained from the GFI and the CADW and IC methods in the limit of zero external electric field.

$\log_{10}T$ (K)	GFI	O^{5+} CADW	IC
4.6	3.20×10^{-11}	3.60×10^{-11}	2.35×10^{-11}
4.8	5.47×10^{-11}	5.03×10^{-11}	4.00×10^{-11}
5.0	5.94×10^{-11}	5.12×10^{-11}	4.43×10^{-11}
5.2	4.85×10^{-11}	4.09×10^{-11}	3.68×10^{-11}
5.4	3.31×10^{-11}	2.76×10^{-11}	2.54×10^{-11}
5.6	2.02×10^{-11}	1.67×10^{-11}	1.56×10^{-11}
5.8	1.14×10^{-11}	9.45×10^{-12}	8.87×10^{-12}
6.0	6.18×10^{-12}	5.11×10^{-12}	4.82×10^{-12}
6.2	3.25×10^{-12}	2.69×10^{-12}	2.54×10^{-12}
6.4	1.68×10^{-12}	1.39×10^{-12}	1.32×10^{-12}
6.6	8.60×10^{-13}	7.09×10^{-13}	6.73×10^{-13}
6.8	4.36×10^{-13}	3.60×10^{-13}	3.42×10^{-13}

that in the high temperature limit the GFI and CADW results are about 10% and 20% larger than the corresponding IC results, respectively. For O^{2+} we see in Table II that the CADW model predicts that the maximum in the DR rate coefficient occurs at a lower temperature than calculated by the IC method. Hence this is opposite to the O^+ case, but agrees with the corresponding maximum-field enhancement assignments in Figs. 1 and 2 above. In the high temperature limit the CADW results are about 8% lower than the corresponding IC results. The O^{3+} results in Table III very much follow the previously discussed O^{2+} data. However, the deviations from the IC results are larger for the currently discussed ion. For O^{2+} and O^{3+} DR takes place through Rydberg series attached to more than one core term. Hence we expect these cases to show some similarities. From Table IV we see that the GFI assigns the maximum value of the rate coefficient to a larger temperature and that the CADW method associates it with a lower temperature than the more sophisticated IC model. We notice that this case gives the largest deviations from the calibration results, i.e., the data obtained using the IC method. This agrees with the discussion of the general features of the O^{4+} ion included in connection with the maximum-field enhancement results above. The configuration-average distorted-wave method will produce a peak value shifted towards lower temperatures due to the averaging over the $2s2p\,(^1P)$ and $2s2p\,(^3P)$ states of the excited O^{4+} ion. From Table V we observe that the maximum rates for O^{5+} as calculated by the GFI and CADW methods are about 34% and 15% larger than the IC results, respectively. The corresponding high-temperature results differ by 27% and 5% from the calibration data. In concluding this comparison we note that all three methods show the expected increasing tendency in the DR rate coefficients as we go along the isonuclear sequence toward higher charge states. We further note that the simple to use Burgess general formula I seems to produce rather reliable DR rate coefficients for the presently studied ions (in the limit of zero external electric fields).

IV. SUMMARY AND CONCLUSIONS

We have presented DR rate coefficients for O^{q+}, $q = 1, \ldots, 5$, calculated in intermediate coupling and configuration-average distorted-wave approximations as well as obtained from the Burgess general formula I and II. By combining the results from the CADW zero field (i.e., not enhanced, but still field ionized) and maximum-field enhancement calculations we were able to explore the two competing effects in the presence of external electric fields, i.e., the increase in the DR rate coefficients due to Rydberg-state mixing and the decrease due to field ionization. In particular, we found that strong fields caused the DR rates to drop by over a factor of 10 at the peak temperature. In general, we stressed the importance of appropriate modeling of environmental effects such as external fields; however, density fluctuations may also be important. Angular-momentum-changing collisions between autoionizing states of the same complex are known to produce a substantial increase in the DR rate coefficients, while collisions involving the excited final states of the recombined ion lead to a decrease in the effective recombination rate.[3] However, since there is no simple way to model density effects in connection with the DR process,[18] we have restricted ourselves to field effects in this paper. We also noted that the configuration-average distorted-wave approximation may be an important tool in the investigation of these effects, although it is necessary to be extremely careful when interpreting the results in "pathological" cases, such as O^{4+}. From the comparison of the CADW and GFII results for the O isonuclear sequence we noted that the GFII predicted, qualitatively, fairly accurate DR rate coefficients. Hence the GFII seems to be appropriate for rough estimates of field-enhanced rates for low-density plasmas and for low charge states. However, we also observed that it was off by up to a factor of 3 at the peak temperature. The Burgess general formula I seems to be more dependable than the second formula. The comparison with the results of the IC and CADW models showed that for the worst case the GFI was off by no more than a factor of 1.5 and that it otherwise deviated from the calibration results by no more than a factor of 1.2.

However, in order to obtain very accurate DR rate coefficient results as well as more detailed information about the impact of the atomic structure on DR cross sections, one is obviously forced to use more sophisticated methods such as, e.g., the IC model[5] (including Rydberg electron transitions) in the field-free limit or an intermediate-coupling distorted-wave approach including field effects[16] when external fields are present.

ACKNOWLEDGMENTS

---

*Permanent address: Manne Siegbahn Institute of Physics, Frescativägen 24, S-104 05 Stockholm, Sweden.

†Present address: Department of Physics, Auburn University, Auburn, Alabama 36849-5311.

[1]Report of the International Atomic Energy Agency Specialists Meeting on Carbon and Oxygen Collision Data for Fusion Plasma Research, Vienna, 1988 [Phys. Scr. T28 (1989)].

[2]V. L. Jacobs, J. Davis, and P. C. Kepple, Phys. Rev. Lett. 37, 1390 (1976).

[3]V. L. Jacobs and J. Davis, Phys. Rev. A 18, 692 (1978).

[4]N. R. Badnell and M. S. Pindzola, Phys. Rev. A 39, 1690 (1989).

[5]N. R. Badnell, J. Phys. B 19, 3827 (1986).

[6]D. C. Griffin, M. S. Pindzola, and C. Bottcher, Phys. Rev. A 31, 568 (1985).

[7]P. F. Dittner, S. Datz, P. D. Miller, P. L. Pepmiller, and C. M. Fou, Phys. Rev. A 35, 3668 (1987).

[8]P. F. Dittner, S. Datz, H. F. Krause, P. D. Miller, P. L. Pep-

miller, C. Bottcher, C. M. Fou, D. C. Griffin, and M. S. Pind-zola, Phys. Rev. A **36**, 33 (1987).

[9]P. F. Dittner, S. Datz, H. F. Krause, P. D. Miller, P. L. Pep-miller, C. M. Fou, Y. Hahn, and I. Nasser, Phys. Rev. A **38**, 2762 (1988).

[10]A. Burgess (private communication).

[11]A. Burgess, Astrophys. J. **141**, 1588 (1965).

[12]Y. Hahn, Adv. At. Mol. Phys. **21**, 123 (1985).

[13]C. Bottcher, D. C. Griffin, and M. S. Pindzola, Phys. Rev. A **34**, 860 (1986).

[14]R. J. Damburg and V. V. Kolosov, J. Phys. B **12**, 2637 (1979).

[15]C. Lanczos, Z. Phys. **68**, 204 (1931).

[16]D. C. Griffin, M. S. Pindzola, and C. Bottcher, Phys. Rev. A **33**, 3124 (1986).

[17]W. L. Wiese, M. W. Smith, and B. M. Glennon, *Atomic Transition Probabilities* (National Standard Reference Data Series, Washington, D.C., 1966).

[18]A. Burgess and H. P. Summers, Astrophys. J. **157**, 1007 (1969).

FIG. 1. (a) CADW zero-field and maximum-field enhancement O^+ dielectronic recombination rate coefficients as a function of the temperature. Displayed are the results for $n_{max} = 10, 20, 200$. (b) The same as in (a) but obtained from the Burgess general formula II. Shown are the results for $n_{max} = 10$, solid curve; 20, dashed curve; and 200, dotted curve.
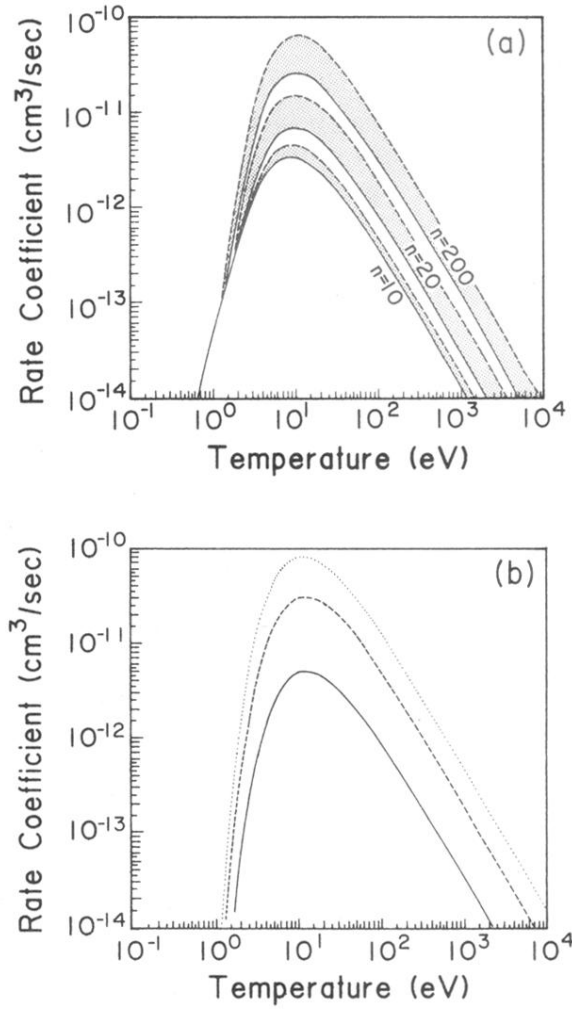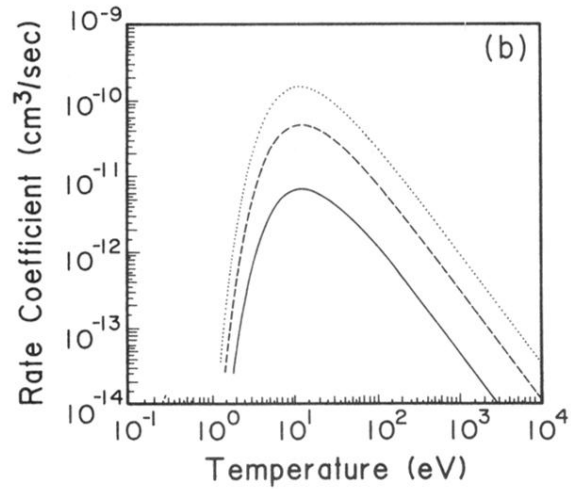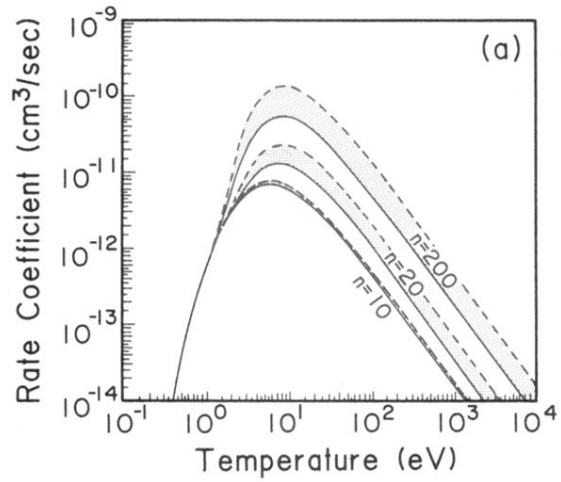
FIG. 2. (a) CADW zero-field and maximum-field enhancement O^{2+} dielectronic recombination rate coefficients as a function of the temperature. Displayed are the results for $n_{max} = 10, 20, 200$. (b) The same as in (a) but obtained from the Burgess general formula II. Shown are the results for $n_{max} = 10$, solid curve; 20, dashed curve; and 200, dotted curve.
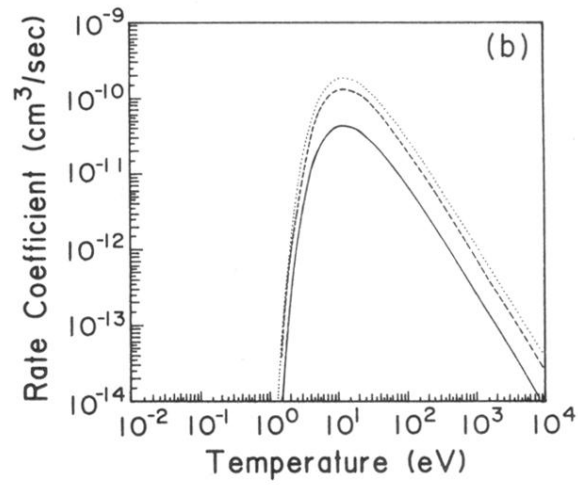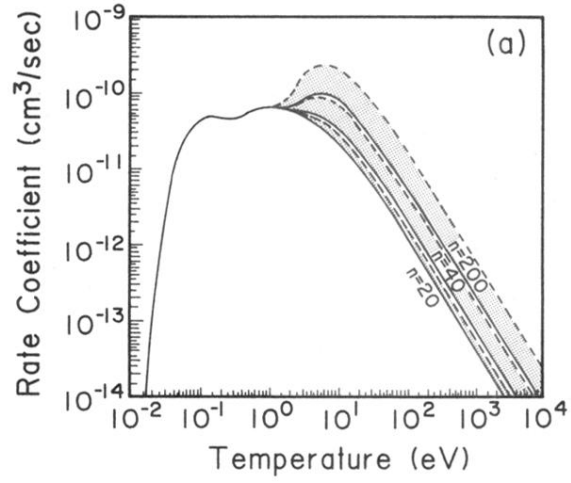
FIG. 3. (a) CADW zero-field and maximum-field enhancement O^{3+} dielectronic recombination rate coefficients as a function of the temperature. Displayed are the results for $n_{max} = 10, 20, 200$. (b) The same as in (a) but obtained from the Burgess general formula II. Shown are the results for $n_{max} = 10$, solid curve; 20, dashed curve; and 200, dotted curve.
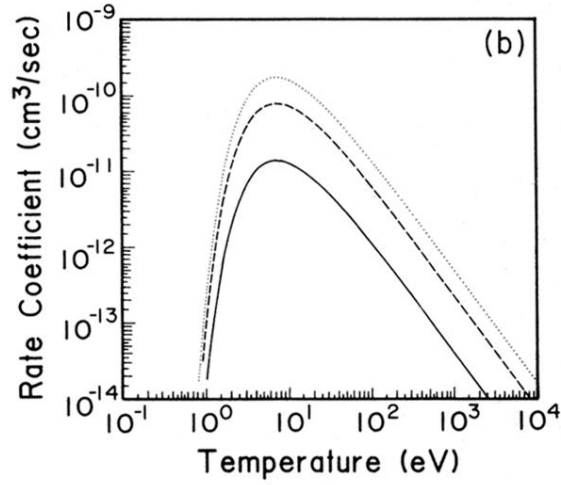
FIG. 4. (a) CADW zero-field and maximum-field enhancement O^{4+} dielectronic recombination rate coefficients as a function of the temperature. Displayed are the results for $n_{max} = 20, 40, 200$. (b) The same as in (a) but obtained from the Burgess general formula II. Shown are the results for $n_{max} = 20$, solid curve; 40, dashed curve; and 200, dotted curve.
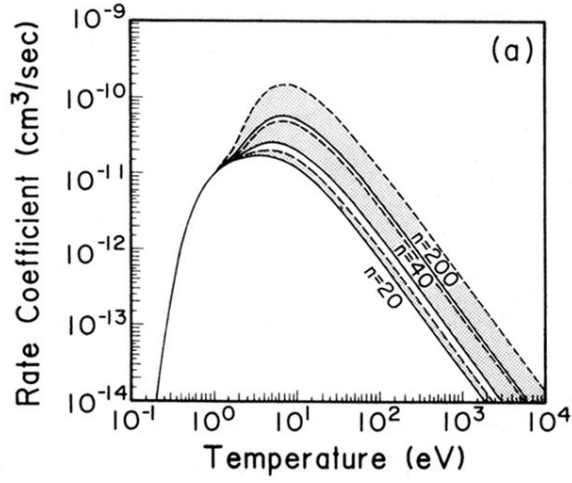
FIG. 5. (a) CADW zero-field and maximum-field enhancement O^{5+} dielectronic recombination rate coefficients as a function of the temperature. Displayed are the results for $n_{max} = 20, 40, 200$. (b) The same as in (a) but obtained from the Burgess general formula II. Shown are the results for $n_{max} = 20$, solid curve; 40, dashed curve; and 200, dotted curve.